Tensile strength of partially filled FFF printed parts: meta modelling

Shahrain Mahmood
School of Mechanical & Systems Engineering, Singapore
A.J. Qureshi
Department of Mechanical Engineering, University of Alberta, Edmonton, Canada, and
Kheng Lim Goh and Didier Talamona
School of Mechanical & Systems Engineering, Singapore and School of Mechanical & Systems Engineering, Australia

Abstract

Purpose – This paper aims to investigate the tensile strength of partially filled fused filament fabrication (FFF) printed parts with respect of cross-sectional geometry of partially filled test pieces. It was reported in the authors' earlier work that the ultimate tensile strength (UTS) is inversely proportional to the cross-sectional area of a specimen, whereas the number of shells and infill density are directly proportional to the UTS with all other parameters being held constant. Here, the authors present an in-depth evaluation of the phenomenon and a parametric model that can provide useful estimates of the UTS of the printed part by accounting for the dimensions of the solid floor/roof layers, shells and infills.

Design/methodology/approach – It was found that partially filled FFF printed parts consist of hollow sections. Because of these voids, the conventional method of determining the UTS via the gross cross-sectional area given by $A = b \times h$, where b and h are the width and thickness of the printed part, respectively, cannot be used. A mathematical model of a more accurate representation of the cross-sectional area of a partially filled part was formulated. Additionally, the model was extended to predict the dimensions as well as the lateral distortion of the respective features within a printed part using input values from the experimental data.

Findings – The result from this investigation shows that to calculate the UTS of a partially filled FFF part, the calculation based on the conventional approach is not sufficient. A new meta-model is proposed which takes into account the geometry of the internal features to give an estimate of the strength of a partially filled printed part that is closer to the value of the strength of the material that is used for fabricating the part.

Originality/value – This paper investigates the tensile strength of a partially filled FFF printed part. The results have shown that the tensile strength of a partially filled part can be similar to that of a solid part, at a lower cost: shorter printing time and lower material usage. By taking into account the geometries within a printed part, the cross-sectional area can be accurately represented. The mathematical model which was developed would aid end-users to predict the tensile strength for a given set of input values of the process parameters.

Keywords Tensile strength, Fused filament fabrication, Additive manufacturing, Meta modelling

Paper type Research paper

1. Introduction

Fused filament fabrication (FFF) has become a common tool to produce functional prototypes as well as end-user products in recent years. The ability to produce elaborated parts without the need for any conventional or intermediate tooling is one of the many advantages of this process. FFF is a complicated process which requires the interaction of various process parameters to achieve the required material strength and dimensional accuracy (Moza *et al.*, 2015). Varying these process parameters have been shown to have an effect on the tensile strength of the printed parts (Ahn *et al.*, 2002; Górski *et al.*, 2013; Lee *et al.*, 2005). With limited knowledge and lack of proper testing equipment, small and medium enterprises possessing FFF printers may not have the necessary information required to produce parts with the desired mechanical properties.

This paper investigates the effects of varying the cross-sectional area (variations in the width and thickness of specimen), number of shells and infill density to the tensile strength of FFF printed parts. According to a recent investigation (Mahmood *et al.*, 2017), it was found that the ultimate tensile strength (UTS) varies inversely with the cross-sectional area, whereas increasing the number of shells and infill density increases the UTS. This paper further develops a mathematical model to predict the tensile force at fracture for FFF printed parts based on the parameters considered.

The FFF printer used in this investigation was the Makerbot Replicator 2X from Makerbot Industries and test specimens were printed with a 1.75 mm diameter Acrylonitrile Butadiene Styrene (ABS) filament. Test specimens were

The current issue and full text archive of this journal is available on Emerald Insight at: **www.emeraldinsight.com/1355-2546.htm**

Rapid Prototyping Journal
23/3 (2017) 524–533

[DOI 10.1108/RPJ-10-2015-0151]

Received 24 October 2015
Revised 12 February 2016
22 April 2016
16 June 2016
Accepted 8 July 2016

printed in an environment where temperature was maintained at 25°C and relative humidity at about 65 per cent. Computer aided design (CAD) models are processed using the Makerbot Desktop software.

2. State of the art

Montero *et al.* (2001), Sood *et al.* (2010), Fatimatuzahraa *et al.* (2011), Ziemian and Sharma (2012) and Onwubolu and Rayegani (2014) have investigated the effects of varying some parameters to the tensile strength of FFF printed parts. The effects of parameters such as raster angle, layer thickness, air gap and build orientation have been investigated with UTS obtained ranging from a minimum of 18.1 MPa to a maximum of 32.6 MPa.

Montero *et al.* (2001) developed a predictive model of the UTS of ABS printed parts as a function of air gap and raster orientation. The mathematical model results yielded an error from 4.4 to 6.3 per cent when compared to actual experimental results.

Onwubolu and Rayegani (2014) created a predictive model that calculates the UTS based on the group method for data handling method. Five parameters (layer thickness, part orientation, raster angle, raster width and air gap) were used in the model. In the investigation, it was concluded that the mathematical model predicts UTS with little deviation from the experimental results for a particular combination of parameters.

Qureshi *et al.* (2015) investigated the effects of variation of 12 process parameters on the UTS of ABS printed parts. The parameters considered in the investigation included component scale, extruder temperature, infill pattern, layer thickness, print speed, print orientation and the number of shells. It was found that component scale, print orientation and number of shells had the most significant effect on the UTS of the printed parts. It was also found that parameters such as extruder temperature, layer thickness and infill pattern had minimal or no significant effect on the UTS of the printed parts.

However, as highlighted by Melenka *et al.* (2015), the investigations mentioned were performed on a commercial 3D printer and not a desktop consumer grade 3D printer. More importantly, specimens used for those investigations were printed with an infill density of 100 per cent, approximating to a solid part. Contrary to solid filled parts, partially filled printed parts consist of voids within its interior structure. Although partially filled printed parts depict lesser strength than solid parts, they have the advantage of significantly lesser build times and material (An *et al.*, 2015), enabling rapid appraisal of a CAD concept. For an ASTM D638 Type IV standard part, with a 10 per cent infill density, it would require about 33 min to print and require approximately 4.5 grams of material. A similar part printed with a 100 per cent infill density requires approximately 58 min and about 8.3 grams of material. It can be seen that printing with a partially filled part requires lesser printing time and material. These numbers become significantly higher for multi-component assemblies. The lesser strength of partially filled parts can be improved by increasing the number of shells (Qureshi *et al.*, 2015).

3. Methodology

A systematic methodology is proposed for investigating and developing a method for allowing a better estimation of the tensile strength of partially filled FFF printed parts comprising the following steps:

1. *Design of experiment*: This step comprises design and setup of a multi-variable experimental setup for production and testing of a test specimen by applying an appropriate design of the experiment method.
2. *Theoretical method for tensile force estimation*: This step comprises generation of the test specimen CAD model; importing and slicing the model with the printer software; and calculation of the peak force for the specimen based on the effective cross-sectional area of a partially filled FFF part, information from the CAD model, print settings and the material property of the filament used.
3. *Experimental evaluation for tensile strength*: This step comprises the following:
   - tensile testing of the printed specimens and geometrical assessment of the cross-sectional area of a partially filled part via coordinate measuring machine (CMM);
   - calculation of UTS based on the effective cross-sectional area of a partially filled FFF part; and
   - validation of the theoretical results in light of the experimental results.
4. *Development of a meta model based on the experimental data*: This section proposes a predictive meta model for calculating the cross-sectional area and maximum tensile force of a partially filled FFF printed part and validation of the meta model results when compared to the experimental data.

4. Design of experiment

The authors' earlier work provided a comprehensive list of the process parameters and their effects on the tensile strength of FFF printed parts (Qureshi *et al.*, 2015). As highlighted by Mahmood *et al.* (2017), the cross section of a FFF printed part comprises solid outer boundaries, support structures and voids within this outer boundary. As such, a new method to calculate the effective cross-sectional area of a FFF printed part is proposed in this investigation.

To focus on the scalability issue, Mahmood *et al.* (2017) considered four parameters: specimen width (b), specimen thickness (h), number of shells (n) and infill density (i). Each of these parameters were assigned with three level of controls as shown in Table I.

Taguchi's design of experiment method was selected as it allows the study on the effect of the four parameters to tensile strength with minimal number of experiments required. According to Taguchi (Phadke, 1989), with four parameters

Table I Parameters with level of controls

Parameter	Symbol	Units	Level 1	Level 2	Level 3
Width	b	mm	10	15	20
Thickness	h	mm	4	6	8
Number of shells	n	–	1	2	3
Infill density	i	%	25	50	75

and three control levels, a L9 orthogonal array is required to evaluate their effect on the tensile strength of the printed parts. A L9 orthogonal array will require nine experimental runs altogether, each independent of the parameters and control levels, with the assumption that no interactions take place between any two parameters. Table II shows the combinations for the four parameters for all the nine experimental runs.

Because of the scaling factor required for investigation, a beam-shaped specimen with uniform rectangular cross section of width, b (10 mm); thickness, h (4 mm); and length, l (150 mm), was selected as the Level 1 control, instead of a dog bone specimen as the dimensions of the specimen would no longer conform to the ISO (2012) standard test part. b and h were varied in accordance with the assigned control level while l was fixed at 150 mm (Figure 1).

Five specimens were printed for each experimental run to ensure for consistency and process reliability of the process, resulting in a total population of 45 test specimens for all nine experimental runs. Specimens were tested for tensile strength until fracture and dimensions of the geometries on the fracture surface were measured using CMM.

5. Theoretical method for force estimation

To theoretically estimate the maximum tensile force at rupture for a partially filled FFF printed part, the cross-sectional area of the part can be estimated directly with the information from the CAD model and the printer software.

The CAD model can be created in any solid modelling environment and then exported to a stereolithography (stl) file format, a format commonly used in the additive manufacturing process. The stl format only reads the surface geometry of the CAD model and not any other attributes associated to the model.

Using the printer's slicing software and the selected process parameters, the software will "slice" the model into horizontal layers and generate the toolpath for printing. The Makerbot Desktop software was used to prepare the stl file for printing. A typical cross section of a partially filled part is shown in Figure 2.

This cross section can be broken down into the respective geometries as shown in Figure 3, a solid floor (h_{floor}) and roof (h_{roof}) layer and outer walls (b_{left} and b_{right}), which depend on the number of shells (n); the interior support structure or infill (diameter, d) printed in rows (R) and columns (C) dependent on the infill density (i). The remaining areas within the part are voids.

Figure 3 shows the number of rows, $R = 5$, and columns, $C = 3$, of the infill. Hence, the effective cross-sectional area of a partially filled FFF part, A', can be estimated by the following equation:

$$A' = (b \times h) - (b' \times h') + \left\{\left(\frac{\pi d^2}{4}\right) \times R \times C\right\} \quad (1)$$

Where

b' = $b - (b_{left} + b_{right})$;
b_{left} and b_{right} = are the outer wall thicknesses;
h' = $h - (h_{floor} + h_{roof})$;
h_{floor} and h_{roof} = are the solid layer thicknesses,
R = number of rows;
C = number of columns and
d = diameter of infill.

Table II Taguchi's L9 orthogonal array matrix

Run	b	h	n	i
1	10	4	1	25
2	10	6	2	50
3	10	8	3	75
4	15	4	2	75
5	15	6	3	25
6	15	8	1	50
7	20	4	3	50
8	20	6	1	75
9	20	8	2	25

Figure 1 CAD model of the test part

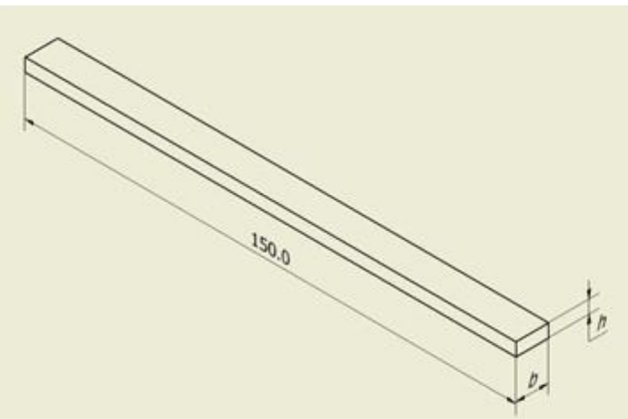

Figure 2 Cross section of a printed part

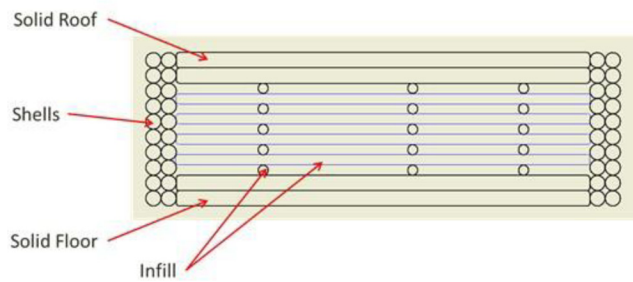

Figure 3 Geometries within a printed part

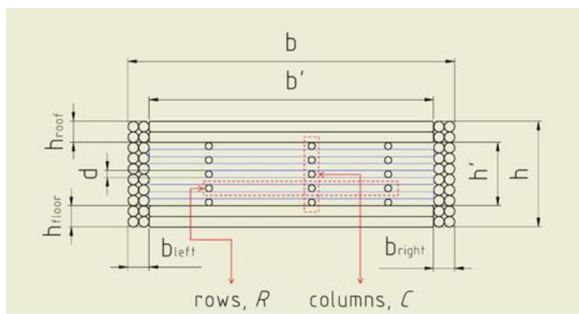

For a standard resolution printer setting, the h_{floor} and h_{roof} thickness is 0.8 mm. The shell width, for $n = 1$, is approximately 0.5 mm, the shell width can then be estimated by $(0.5 \times n)$ mm. The overall shell width for $n > 1$ is affected by the inset distance multiplier value, a multiplier of layer width. This defines the amount of overlap or gap between adjacent shells. This value was set at 0.7, meaning that there was a slight overlap between any two adjacent shells. The infill diameter, d, was dependent on the layer width ratio, that is, the ratio of extrusion width to the layer thickness, given as 1.48148 from the software. Hence, with a layer thickness of 0.2 mm, $d = 0.296$ mm. With an infill density of 10 per cent, R and C can be counted directly from the software, in this case, $R = 12$ (counted from the number of layers to be printed for the infill pattern) and $C = 2$ (the number of infill across the fracture surface) with the assumption that the fracture will occur along the line as shown in Figure 4, based on the hollow cross section where the cross-sectional area of the specimen was the smallest.

With this methodology, the theoretical effective cross-sectional area, A'_{th}, of a partially filled part for Run 1 can be calculated as $A'_{th} = 21.7$ mm^2, using equation (1), where $n = 1$, $i = 25$ per cent, $R = 8$ and $C = 6$, and the theoretical force at rupture, $F_{th} = 694.4$ N, based on the nominal UTS (UTS_{nom}) of 32.0 MPa, derived from testing solid ABS materials to rupture at a displacement rate of 1 mm/min (Bai *et al.*, 2007). Table III summarizes the theoretical values for the respective geometries, A'_{th}, and peak force, F_{th}, calculated for each of the experimental run as seen in Table II. These values were based on the information from the CAD model and the printer's "slicing" software, Makerbot Desktop.

Thus, with this theoretical method, the tensile force can be estimated without the need to perform any mechanical testing. The tensile force can be found based on a known tensile strength of the material used and the effective cross-sectional area using the dimensions of the CAD model and printer settings from the slicing software. All consumer grade FFF printers use a common "G-code" generator, in accordance with the NIST RS274NGC G-code Standard, for slicing and generating the toolpath for printing; this force estimation method can be applied to any slicing software across different machine manufacturers.

Figure 4 Print preview of the part with a standard resolution print setting

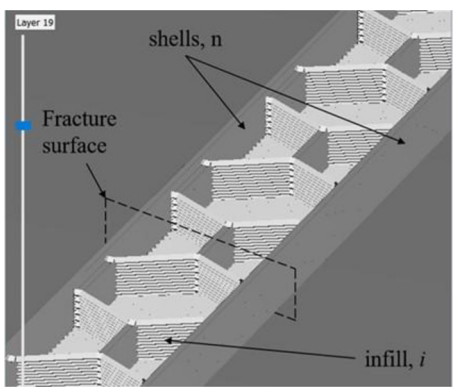

6. Experimental evaluation

To have a more accurate representation of the effective cross-sectional area, and to correlate the results with the theoretical method presented above, the geometries within the cross section, taken from a fractured surface, were measured using a CMM.

From Figure 5, the cross section of the fractured surface for a Run 1 specimen, it can be seen that $n = 1$, $R = 7$ and $C = 6$. The numbers of R, horizontal infills, and C, vertical infills, were deduced by counting the number of infills within the specimen. The infill diameter, d, was measured at five random locations with the average diameter used for calculating the overall experimental cross-sectional area, A'_{exp}. The dimensions for the various geometries and the calculated A'_{exp} and the peak force, F_{exp}, recorded are shown in Table IV.

It can be seen that percentage differences between A'_{exp} and A'_{th} ranged from +4.2 to +14.0 per cent, with $A'_{exp} < A'_{th}$, across all the experimental runs. This variation between A'_{exp} and A'_{th} can be attributed to several factors such as deformation of extruded layers during tensile testing as the experimental values were based on measurements taken after fracture, whereas the theoretical values were purely from the CAD model and printer settings, the effects of air gaps between extruded layers and the dimensional accuracy of printing (Moza *et al.*, 2015). Similarly, F_{exp} was smaller as compared to F_{th} for most of the experimental runs with a percentage difference ranging from −8.9 to +3.8 per cent.

The UTS were calculated based on A_{exp}, and Figure 6 shows the population distribution of the tensile strength for all 45 specimens. The minimum and maximum tensile strength recorded were 31.9 and 39.0 MPa, respectively, with a population mean, $\mu = 34.28$ MPa, and standard deviation,

Table III Theoretical values for the geometries, effective cross-sectional area and force based on $UTS_{nom} = 32$ MPa

Run	h_{floor} (mm)	h_{roof} (mm)	b_{left} (mm)	b_{right} (mm)	n	d (mm)	R	C	A'_{th} (mm^2)	F_{th} (N)
1	0.8	0.8	0.5	0.5	1	0.29	8	6	21.70	694.4
2	0.8	0.8	1.0	1.0	2	0.29	15	8	32.78	1,049
3	0.8	0.8	1.5	1.5	3	0.29	21	9	47.90	1,533
4	0.8	0.8	1.0	1.0	2	0.29	8	13	35.96	1,151
5	0.8	0.8	1.5	1.5	3	0.29	15	8	45.18	1,446
6	0.8	0.8	0.5	0.5	1	0.29	21	12	47.33	1,515
7	0.8	0.8	1.5	1.5	3	0.29	8	15	47.46	1,519
8	0.8	0.8	0.5	0.5	1	0.29	15	20	56.36	1,804
9	0.8	0.8	1.0	1.0	2	0.29	21	10	58.91	1,885

Figure 5 Image of the cross section of a partially filled part (Run 1)

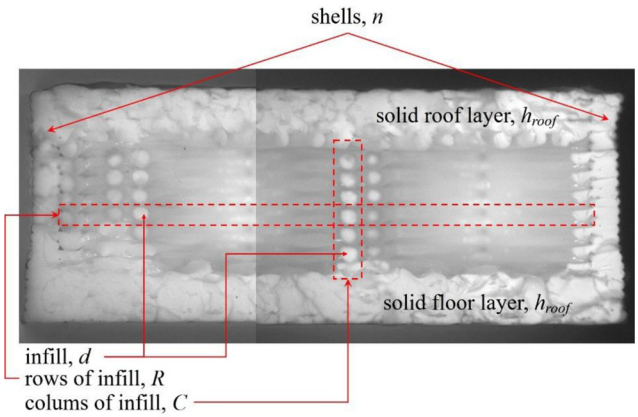

Figure 6 Histogram of the number of specimens versus UTS

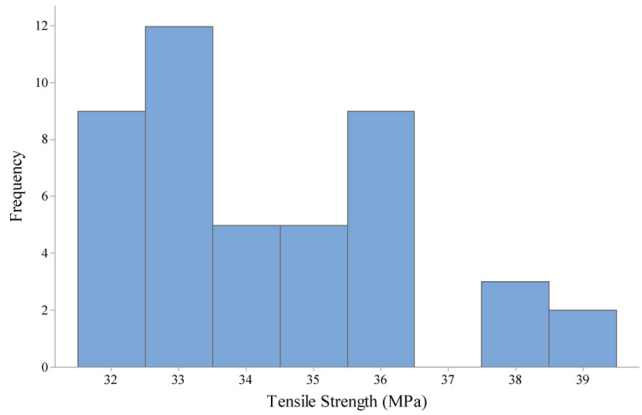

σ = 1.96 MPa. Almost all the specimens were within $\pm 1\sigma$ except for specimens in Run 4 which were within $\pm 2\sigma$.

The results obtained are consistent to the tensile strength of the ABS material, reported by Bai *et al.* (2007) as compared to the results using the gross cross-sectional area of $A = (b \times h)$ (Mahmood *et al.*, 2017). This represents a more accurate expression for the UTS of a partially filled FFF printed part. From Figure 7, it can be seen that with the new formulation being proposed, which takes into account the scaling effects on the overall strength of the printed part, the UTS of the test specimens were not significantly affected by variations in b, h, n and i.

From Table V, h is ranked the highest from the response table for SN ratio and means, followed by b, i and n. The variations in h had the most significant effect on the UTS, however, compared to the recent findings (Mahmood *et al.*, 2017); the delta had decreased significantly by about 70 per cent from 3.02 MPa to 0.88 MPa (SN ratio) and about 30 per cent from 5.16 MPa to 3.54 MPa (means). Similarly, changes in b, n and i had very little effect on the UTS, by about 1 per cent change for SN ratio and 4 per cent for means.

The experimental results clearly show that the effect of scalability to the tensile strength of the printed part, as reported earlier (Qureshi *et al.*, 2015; Mahmood *et al.*, 2017), can be compensated and taken into account when calculated based on A', consistent with any conventional manufacturing process whereby the strength of a manufactured part will not be affected by any scaling factor.

7. Order of magnitude estimates of the nominal cross-sectional area

A mathematical model that predicts the initial structure dimensions and shapes within the cross section of the printed part has been developed. The motivation is to connect the overall dimensions of the printed part to the dimensions of the geometries in a consistent manner that can allow for insights into the scalability of the FFF printed parts, as well as the underlying mechanics of deformation that led to the changes in the structure of these geometries.

Structural deformation of a material takes place whenever it is subjected to any form of load. If an axial load is applied to the printed form, the cross-section areas of the geometries will be altered according to the material response to Poisson's effect. It has to be noted that only the external dimensions (b and h) could be measured before mechanical testing and that the internal dimensions (h_{floor}, h_{roof}, b_{left}, b_{right} and d) were measured after rupture. Thus, equation (1) is a first approximation of the effective cross-sectional area, A'. This equation was refined by introducing correction coefficients to become:

$$A'_{nom} = bh - [\{b - \beta(b_{left} + b_{right})\} \times \{h - \eta(h_{floor} + h_{roof})\}] + \left\{\frac{\pi}{4}(\delta_b d \times \delta_h d) \times R \times C\right\} \quad (2)$$

Table IV Measured values for geometries and the calculated A'_{exp} and F_{exp}

Run	h_{floor} (mm)	h_{roof} (mm)	b_{left} (mm)	b_{right} (mm)	n	d_{ave} (mm)	R	C	A'_{exp} (mm^2)	F_{exp} (N)
1	0.82	0.68	0.48	0.47	1	0.26	7	6	19.65	706.9
2	0.85	0.72	0.77	0.86	2	0.32	13	8	31.28	1,005
3	0.75	0.73	1.43	1.27	3	0.30	20	9	45.89	1,502
4	0.81	0.71	0.89	0.85	2	0.24	7	13	31.25	1,196
5	0.83	0.83	1.36	1.28	3	0.25	13	8	41.26	1,348
6	0.85	0.76	0.54	0.63	1	0.22	20	12	40.72	1,391
7	0.79	0.72	1.19	1.35	3	0.27	7	15	42.40	1,507
8	0.86	0.78	0.49	0.46	1	0.26	13	21	51.24	1,762
9	0.81	0.79	0.93	0.84	2	0.25	20	10	52.91	1,731

Figure 7 Main effect plots for (a) SN ratios and (b) Means

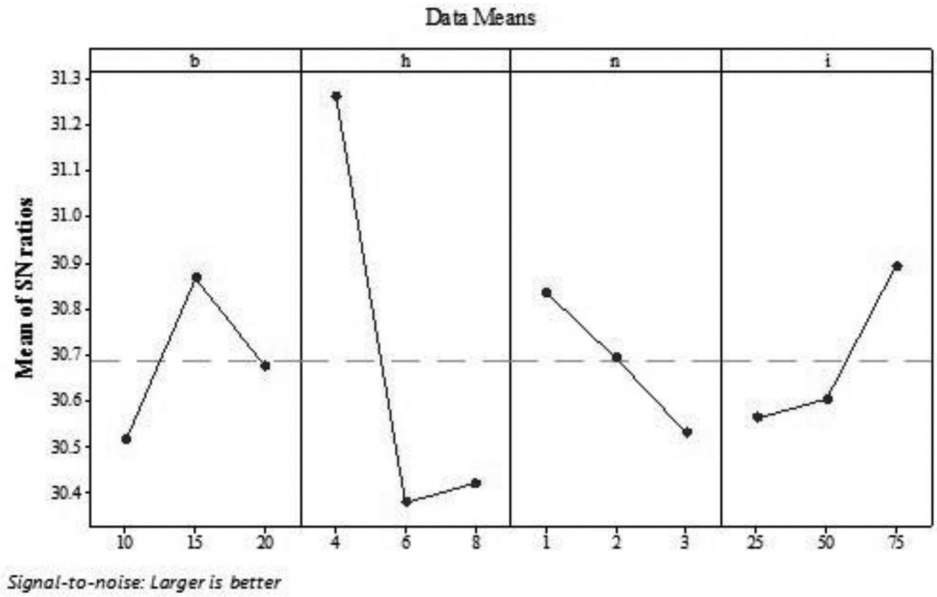

(a)

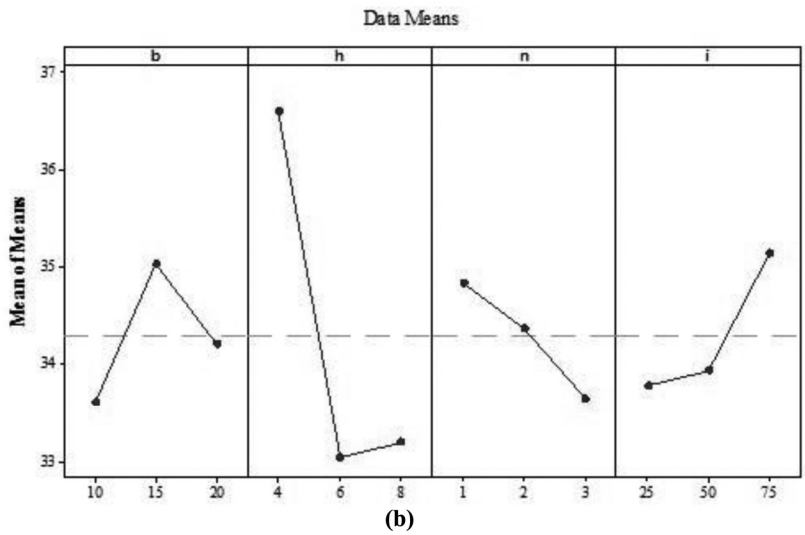

(b)

Table V Response table for SN ratios and means of the UTS, based on A'_{exp}

	Response table for SN ratio					Response table for means			
Level	***b***	***h***	***n***	***i***	**Level**	***b***	***h***	***n***	***i***
1	30.52	31.26	30.84	30.56	1	33.60	36.59	34.83	33.78
2	30.87	30.38	30.69	30.60	2	35.03	33.05	34.27	33.93
3	30.68	30.42	30.53	30.89	3	34.21	33.20	33.65	35.13
Delta	0.35	0.88	0.30	0.33	Delta	1.43	3.54	1.19	1.35
Rank	2	1	4	3	Rank	2	1	4	3

where β, η, δ_b and δ_h are the correction coefficients to account for the changes to the shell width, the solid floor and roof layers thicknesses and the horizontal and vertical infill diameter, respectively.

The correction coefficients were evaluated using a minimization algorithm according to:

$$\min\left(UTS_{nom} - \frac{F_{exp}}{A'_{nom}}\right) = 0 \quad (3)$$

where UTS_{nom} = 32.0 MPa.

Using equation (3), with R, C and the measured data of b, b_{left}, b_{right}, h, h_{floor}, h_{roof} and d, the values for β, η, δ_b and δ_h can be computed and are shown in Table VI. Physically, these results lend to insights into the relationship between the initial and final dimension and shape of the geometries. In particular, $\eta > 1$ is consistent with the expectation that the initial floor and roof thicknesses were greater than those measured in the ruptured specimens, whereas $\beta < 1$ shows that the initial shell widths were smaller than those in the ruptured specimens. As for the infill, the initial geometry appeared to be elliptic with the long axis, $\delta_b < 1$, in the horizontal direction and short axis, $\delta_h > 1$, in the vertical direction. This structural distortion of the infill probably occurred during the manufacturing stage, when the subsequent layers were laid down.

Table VI Parameters of the corrected nominal cross-sectional area, A'_{nom} [equation (2)]

Parameters	Values
β	0.90
η	1.21
δ_b	0.84
δ_h	1.05

Figure 8 shows the graphs of the mechanical properties versus cross-sectional area to illustrate the scalability effects. Figure 8(a) compares the plots of F_{exp} versus A'_{nom} and F_{th} versus A'_{nom}. The graph clearly shows that F_{exp} is in good agreement with F_{th}. Figure 8(b) compares the plots of the UTS versus A'_{nom} and A with reference line UTS_{nom} = 32 MPa. This analysis reveals that the UTS obtained by computing (F_{exp}/A'_{nom}) yielded a much closer agreement with UTS_{nom} when compared to the UTS obtained by computing (F_{exp}/A) (Mahmood *et al.*, 2017). In particular, the UTS of the former plot cluster very tightly about UTS_{nom}, with minimum and maximum values of 30 and 35 MPa, respectively, which falls within the range of values obtained from equation (1). This is consistent with the expectations as equation (2) provides further refinement to equation (1) by accounting for the correction coefficients β, η, δ_b and δ_h. It can be seen that the effective cross-sectional area of a partially printed part, A', is appreciably smaller when compared to the gross cross-sectional area of $A = (b \times h)$.

8. Mathematical meta-modelling

Meta-modelling of FFF processes have been actively investigated using various techniques such as the artificial neural network, regression analysis and generic programming (Garg *et al.*, 2014) with satisfactory results. A mathematical meta-model (Simpson *et al.*, 2001) based on the control and geometrical parameters of an order two was fitted using Mathematica for comparison between the theoretical, experimental and statistical models. This function was used to develop a mathematical model for the

Figure 8 Scalability plots of the (a) F_{exp} and F_{th} versus A'_{nom} and (b) UTS versus A'_{nom} and A with reference UTS_{nom} = 32.0 MPa

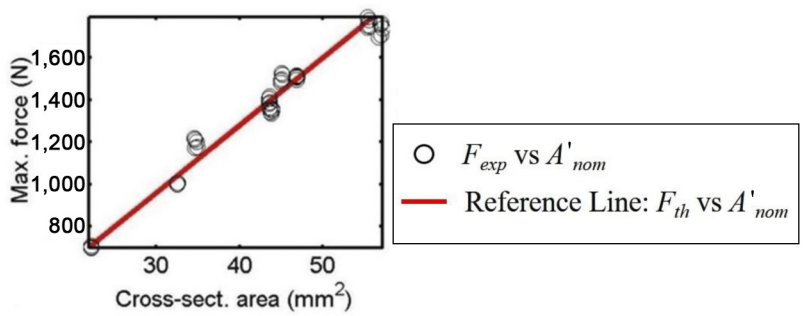

(a)

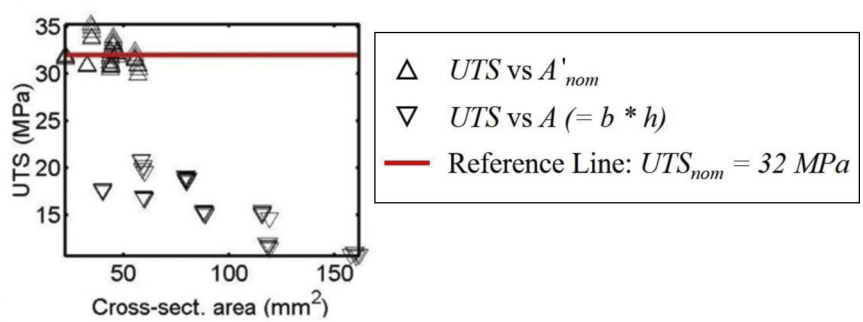

(b)

estimation of the cross-sectional area, tensile strength and tensile force expressed in terms of some or all of the process parameters, b, h, n and i. The meta-model is composed of two parts, a geometrical part that describes the relationship between the control parameters and the cross-section geometry (Section 8.1) resulting in a meta model for tensile strength (Section 8.2), and an expression relating the tensile force to the cross-sectional area of a partially filled FFF part (Section 8.3).

8.1 Geometric meta-model

For the geometries shown in Figure 3, a meta-model between the input parameters b, h, n and i and geometric properties is made. This is specific to an infill pattern. Equation (4) shows the fitted relationship for h_{floor} and the parameters:

$$h_{floor} = \frac{10.51}{b} + \frac{9.33}{h} - \frac{117.59}{(b \times h)} - 0.03h + \frac{27.56}{i} - \frac{362.90}{(h \times i)} + \frac{2995.93}{(b \times h \times i)} \quad (4)$$

This process was repeated for the other geometries. Thus, these equations can be used to predict the values of h_{floor}, h_{roof}, b_{left}, b_{right} and d for any given set of values of b, h, n and i within the limits of the experimentally determined values of b, h, h_{floor}, h_{roof}, b_{left}, b_{right} and d. By substituting the parameters of Run 1 into equation (4), h_{floor} = 0.800 mm (theoretical), but as the measured value was h_{floor} = 0.822 mm (experimental), the difference was 0.022 mm, with a percentage change of approximately 2.7 per cent. Table VII summarizes the mathematical model for the geometries and the percentage variation range between the experimental values to the model output.

The meta model for the cross-sectional area, A'_{mod}, can then be calculated without the need for any physical measurement. The information for b and h is obtained from the CAD model, whereas n and i are the required process parameters for printing. The percentage variation between A'_{exp} and A'_{mod} was within a range from +0.5 to +2.7 per cent across all nine experimental runs (Table VIII). However, the percentage difference between A'_{exp} and A'_{th} showed a larger variation, from +4.2 to +14.0 per cent. This larger variation can be explained by the deformation of the ABS material during mechanical testing as explained in Section 7.

8.2 Meta-model for tensile strength, UTS_{mod}

A meta model for the tensile strength was developed in a similar manner. The UTS was calculated based on the peak force recorded against A'_{exp} and A'_{mod}. Table VIII summarizes the UTS calculated for all the cross-sectional area considered. For Run 1, with an average tensile force of F_{ave} = 706.9 N over five specimens, the experimental UTS calculated was UTS_{exp} = 35.97 MPa, whereas UTS_{mod} = 36.46 MPa. This represented a percentage difference of about −1.3 per cent between the experimental data and the model. Overall, the percentage difference ranged from −2.8 to −0.5 per cent, with the experimental values smaller than the model output, for all the experimental runs. This shows that there is little variation between the experimental results and the model output for the UTS. Table VIII shows the comparison between UTS_{exp} and UTS_{mod} across all experimental runs.

8.3 Meta-model for maximum tensile force, F_{mod}

Similarly, a model for the maximum tensile force was also developed. The maximum tensile force model can be represented by the following equation:

$$F_{mod} = \left(\frac{UTS_{nom} \times A'_{mod}}{0.918}\right) \quad (5)$$

Where UTS_{nom} = 32.0 MPa.

Equation (5) can be used to predict the maximum tensile force for a given A'_{mod}. Using the parameters for Run 1 (A'_{mod} = 19.39 mm^2), we find F_{mod} = 675.9 N, whereas the experimental force recorded F_{exp} = 706.9 N. This reveals a percentage difference of 4.3

Table VII Meta model for the various geometries

Mathematical model	% Variation range
$h_{floor} = \frac{10.505}{b} + \frac{9.331}{h} - \frac{117.593}{(b \times h)} - 0.028h + \frac{27.56}{i} - \frac{362.90}{(h \times i)} + \frac{2995.93}{(b \times h \times i)}$	2.7 to 5.4
$h_{roof} = \frac{7.696}{b} + \frac{11.199}{h} - \frac{141.035}{(b \times h)} - 0.032h + \frac{39.222}{i} + \frac{535.069}{(h \times i)} + \frac{4476.21}{(b \times h \times i)} + 0.067n$	−1.1 to 1.9
$b_{left} = -\frac{17.71}{b} - \frac{1.02}{h} + \frac{45.22}{(b \times h)} + 0.134h - \frac{14.13}{i} + \frac{82.66}{(h \times i)} + 0.79n - (0.02bn)$	−5.7 to −2.3
$b_{right} = -\frac{3.636}{b} - 0.0283b + \frac{4.276}{h} + 0.099h - \frac{9.616}{i} - \frac{0.435i}{(b \times h)} - \frac{0.026b}{(h \times n)} + 0.383n$	−2.3 to 1.5
$d = \frac{10.943}{b} + \frac{1.241}{h} - \frac{34.947}{(b \times h)} - 0.099h + 0.0025bh + 0.00012bh^2$	0.2 to 3.6
$R = \frac{307.573}{b} - 2.078b + \frac{137.702}{h} - \frac{2049.158}{(b \times h)} - 0.741h + 0.316bh - \frac{246.081}{i} + \frac{1399.112}{(h \times i)}$	0
$C = \frac{278.434}{b} + 0.898b + \frac{15.374}{h} - \frac{1494.654}{(b \times h)} - 2.34h - \frac{10.2}{i} + 0.083i + \frac{41.901}{(h \times n)}$	0

Table VIII Summary of the UTS based on the experimental and model data

	Experimental			Model	
Run	F_{ave} (N)	A'_{exp} (mm^2)	UTS_{exp} (MPa)	A'_{mod} (mm^2)	UTS_{mod} (MPa)
1	706.9	19.65	35.97	19.39	36.46
2	1,005	31.28	32.11	30.84	32.57
3	1,502	45.89	32.74	45.64	32.92
4	1,196	31.25	38.29	30.83	38.81
5	1,348	41.26	32.66	40.68	33.13
6	1,391	40.72	34.16	39.63	35.1
7	1,507	42.40	35.54	42.05	35.84
8	1,762	51.24	34.38	50.38	34.97
9	1,731	52.91	32.71	52.54	32.95

per cent between the F_{exp} and F_{mod}, with $F_{exp} > F_{mod}$ for this run. For all the experimental runs, the percentage difference between F_{exp} and F_{mod} ranged from −7.0 to +10.1 per cent.

9. Discussion

The cross-sectional area of a partially FFF printed part consists of various geometries as shown in Figure 2. These geometries were identified, and the dimensions were recorded based on the information from the slicing software. A new method to calculate the effective cross-sectional area of a partially filled FFM printed part, A', equation (1), was developed. It was found that the UTS calculated was a more accurate reflection of the tensile strength of a FFF printed part, although there was still a variation of about 18 per cent for the UTS calculated across all the 45 specimens as compared to a variation of around 50 per cent (Mahmood *et al.*, 2017), for the same specimens, when using the gross cross-sectional area of $A = (b \times h)$, where b and h are measured dimensions before fracture. The variation in the tensile strength, by 18 per cent, can be attributed to the deformation of the extruded layers during the tensile testing, as shown in the earlier section (Section 7), which affects the overall cross-sectional area, A', of a printed part. The results obtained have shown that the UTS of a partially filled FFF printed parts are not affected by any scaling factor unlike earlier reported (Qureshi *et al.*, 2015).

A meta-model of the relationship between the parameters b, h, n, i and force was developed for the tensile strength of FFF printed parts. With the proposed model, end-users would be able to estimate the peak force applied at fracture of a printed part without the need to physically print and perform the required tests on specimens. Therefore, end-users are able to decide on the combination of the input parameters to achieve the required the tensile strength of any printed part. With this model, it was found that the variation between the theoretical and model data ranged from −11.3 to +6.5 per cent.

This variation could be explained by the fact that for the results for all the geometries were lesser in the modelling data as compared to the theoretical data. Furthermore, the geometries were measured after fracture, and structural deformation occurs when subjected to any form of load; hence, the dimensions of the geometries before fracture would be assumed to be larger than that of the measured dimensions.

References

Ahn, S.-H., Montero, M., Odell, D., Roundy, S. and Wright, P.K. (2002), "Anisotropic material properties of fused deposition modeling ABS", *Rapid Prototyping Journal*, Vol. 8 No. 4, pp. 248-257.

An, A., Habib, M.A. and Khoda, B. (2015), "Resource based process planning for additive manufacturing", *Computer-Aided Design*, available at: http://dx.doi.org/10.1016/j.cad.2015.03.006

Bai, X., Isaac, D.H. and Smith, K. (2007), "Reprocessing Acrylonitrile-butadiene-styrene plastics: structure – property relationships", *Polymer Engineering and Science*, Vol. 47 No. 2, pp. 120-130.

Fatimatuzahraa, A.W., Farahaina, B. and Yusoff, W.A.Y. (2011), "The effect of employing different raster orientations on the mechanical properties and microstructure of Fused Deposition Modeling parts", *ISBEIA 2011 - 2011 IEEE Symposium on Business, Engineering and Industrial Applications*, Langkawi, pp. 22-27.

Garg, A., Tai, K. and Savalani, M.M. (2014), "State-of-the-art in empirical modelling of rapid prototyping processes", *Rapid Prototyping Journal*, Vol. 20 No. 2, pp. 164-178, available at: www.emeraldinsight.com/10.1108/RPJ-08-2012-0072

Górski, F., Kuczko, W. and Wichniarek, R. (2013), "Influence of process parameters on dimensional accuracy of parts manufactured using fused deposition modelling technology", *Advances in Science and Technology – Research Journal*, Vol. 7 No. 19, pp. 27-35, available at: www.astrj.pollub.pl/abstracted.php?level=5&ICID=1062340 (accessed 10 October 2014).

ISO (2012), "ISO 527-1:2012: plastics - determination of tensile properties", *Part 1 - General Principles*.

Lee, B.H., Abdullah, J. and Khan, Z.A. (2005), "Optimization of rapid prototyping parameters for production of flexible ABS object", *Journal of Materials Processing Technology*, Vol. 169 No. 1, pp. 54-61.

Mahmood, S., Qureshi, A.J., Goh, K.L. and Talamona, D. (2017), "Tensile strength of partially filled fdm printed components: experimental results", *Rapid Prototyping Journal*, Vol. 23 No. 1.

Melenka, G.W., Schofield, J.S., Dawson, M.R. and Carey, J.P. (2015), "Evaluation of dimensional accuracy and material properties of the makerbot 3D desktop printer", *Rapid Prototyping Journal*, Vol. 21 No. 5, pp. 618-927.

Montero, M., Roundy, S. and Odell, D. (2001), "Material characterization of fused deposition modeling (FDM) ABS by designed experiments", *Proceedings of Rapid Prototyping & Manufacturing Conference*, pp. 1-21, available at: http://ode11.com/publications/sme_rp_2001.pdf (accessed 6 December 2014).

Moza, Z., Kisakis, K., Kechagias, J. and Vaxevanidis, N.M. (2015), "Medical applications of 3D printing-A dimensional accuracy investigation of low cost 3D printing", *International Conference on Food and Biosystems Engineering*, May.

Moza, Z., Kitsakis, K., Kechagias, J. and Mastorakis, N. (2015), "Optimizing Dimensional Accuracy of Fused Filament Fabrication using Taguchi Design", *14th International Conference on Instrumentation, Measurement, Circuits and Systems*, *Salerno*, pp. 110-114.

Onwubolu, G.C. and Rayegani, F. (2014), "Characterization and optimization of mechanical properties of ABS Parts manufactured by the fused deposition modelling process", *International Journal of Manufacturing Engineering*, pp. 1-13, available at: www.hindawi.com/journals/ijme/2014/598531/

Phadke, M.S. (1989), *Quality Engineering Using Robust Design*.

Qureshi, A.J., Mahmood, S., Wong, W.L.E. and Talamona, D. (2015), "Design for scalability and strength optimisation for components created through FDM process", *Proceedings of the 20th International Conference on Engineering Design (ICED2015)*, *Milan*, *27-30* July, pp. 255-266.

Simpson, T.W., Poplinski, J.D., Koch, P.N. and Allen, J.K. (2001), "Metamodels for computer-based engineering design: survey and recommendations", *Engineering With Computers*, Vol. 17 No. 2, pp. 129-150.

Sood, A.K., Ohdar, R.K. and Mahapatra, S.S. (2010), "Parametric appraisal of fused deposition modelling process using the grey Taguchi method", *Proceedings of the Institution of Mechanical Engineers, Part B: Journal of Engineering Manufacture*, Vol. 224 No. 1, pp. 135-145, available at: http://pib.sagepub.com/lookup/doi/10.1243/09544054JEM1565 (accessed 14 December 2014).

Ziemian, C. and Sharma, M. (2012), "Anisotropic mechanical properties of ABS parts fabricated by fused deposition modelling", *Mechanical Engineering*, p. 23, available at: http://cdn.intechopen.com/pdfs/35261/InTech-Anisotropic_mechanical_properties_of_abs_parts_fabricated_by_fused_deposition_modelling.pdf

Further reading

Bellini, A. and Guceri, S. (2003), "Mechanical characterization of parts fabricated using fused deposition modelling", *Rapid Prototyping Journal*, Vol. 9 No. 4, pp. 252-264.

Corresponding author

Shahrain Mahmood can be contacted at: Shahrain.Mahmood@newcastle.ac.uk